ACS Photonics

pubs.acs.org/journal/apchd5

Article

Interfacial Molecular Engineering for Efficient Sn Perovskite Light-Emitting Diodes

Published as part of ACS Photonics special issue "Rising Stars in Photonics".

Seok Joo Yang,[§] Dharini Varadharajan,[§] Kagachi Tateno,[§] Yu-Ting Yang, Jeong Hui Kim, Kevin R. Pedersen, Sung-Doo Baek, Hanjun Yang, Aidan H. Coffey, Kenneth R. Graham, Bryan W. Boudouris, and Letian Dou*

Cite This: *ACS Photonics* 2024, 11, 4941−4947

Read Online

ACCESS | Metrics & More | Article Recommendations | Supporting Information

ABSTRACT: In recent years, perovskite light-emitting diodes (PeLEDs) have demonstrated exceptional potential, achieving high external quantum efficiencies (EQEs) exceeding 20%. However, these advancements have primarily focused on visible colors, and toxic elements such as Pb are used in these devices. Tin (Sn) perovskites with a narrow band gap of nearly 1.3 eV present a promising candidate for lead-free near-infrared PeLEDs. Nonetheless, Sn oxidation and high defect density from fast crystallization are still hurdles to overcome. This study investigates the impact of a newly synthesized ethylenedioxythiophene (EDOT)-based conjugated organic ligand on Sn-based PeLEDs, aiming to enhance device performance by reducing the defect density and Sn oxidation. The EDOT-treated PeLED device achieves a high EQE of 6.4% and exhibits stable electroluminescence spectra, demonstrating the potential of ligand treatments in optimizing Sn-based PeLEDs.

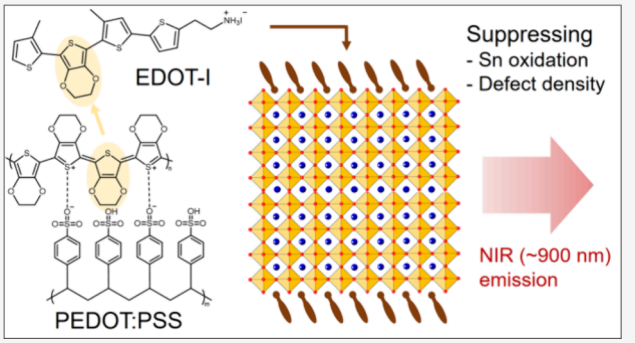

KEYWORDS: *conjugated organic ligand, lead-free perovskites, Sn oxidation, NIR emission, PeLEDs, grain size distribution, energy level, energy funneling*

INTRODUCTION

Metal halide perovskites (MHPs) have been emerging as one of the most promising optoelectronic materials due to superior advantages such as their low-cost-fabrication via solution processing,[1] tunable band gap,[2] balanced charge transport properties with long diffusion lengths,[3] and high photoluminescence quantum yields (PLQYs).[4] All of these are imperative for next-generation optoelectronic applications. Due to the high color purity with narrow emission spectra and wide-ranged color tunability from violet to near-infrared (NIR) wavelengths, MHPs have been widely studied in light-emitting diodes (LEDs).[4] In recent years, efficient perovskite light-emitting diodes (PeLEDs) with high external quantum efficiencies (EQEs) of over 20% have been reported.[1,4−7] However, recent studies have mainly recorded the efficient and color-stable PeLEDs in the three primary colors of red, green, and blue emission (RGB).[8−10] On the other hand, the investigation into NIR PeLEDs is much less explored than their RGB-color counterparts. NIR LEDs are also of great interest for diverse applications including night vision,[11] optogenetics,[12] bioimaging,[13] and optical communications.[14] In order to achieve long-wavelength NIR emission (~900 nm), tin (Sn)-based perovskites have been recently explored due to their narrow band gap (~1.3 eV) and high hole mobilities.[15−18] Furthermore, less toxic Sn perovskites have received great attention as a replacement for lead-based perovskites, which are harmful to the environment ecosystem and human health.[19]

Despite these efforts, the device performance of Sn-based PeLEDs is still lagging behind the counterparts of lead-based PeLEDs,[20−22] mainly attributed to the high defect density from the fast crystallization rate due to their strong Lewis acidity.[22−26] Moreover, facile Sn oxidation from Sn^{2+} to Sn^{4+} at grain boundaries can lead to serious nonradiative recombination in Sn perovskites that degrades electrical properties such as diffusion length and recombination lifetime.[27−31] Therefore, reducing the defect density and Sn oxidation is crucial for efficient Sn-based PeLEDs. Herein, we report a newly designed ethylenedioxythiophene (EDOT)-

Received: August 7, 2024
Revised: October 3, 2024
Accepted: October 10, 2024
Published: October 19, 2024

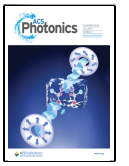

Downloaded via PURDUE UNIV on December 31, 2024 at 18:53:34 (UTC).
See https://pubs.acs.org/sharingguidelines for options on how to legitimately share published articles.

ACS Publications

© 2024 American Chemical Society

based conjugated organic ligand for efficient Sn-based PeLEDs. EDOT has a suitable energy level for efficient charge injection and good adhesion with the PEDOT:PSS layer, which suppresses Sn oxidation and prevents defect formation. As a result, we achieved a high EQE of 6.4% with stable electroluminescence (EL) spectra in the EDOT-treated Sn-based PeLED. These findings create a molecular design template for efficient Sn-based PeLEDs by tuning energy levels and suppressing defect density and Sn oxidation.

EXPERIMENTAL SECTION

Materials. Details on the synthesis of EDOT are noted in the Supporting Information. 2-(3‴,4′-Dimethyl-[2,2′:5′,2″:5″,2‴-quaterthiophen]-5-yl)ethan-1-aminium (4Tm) iodide was synthesized following the previous report.[32] Formamidinium iodide (FAI), 2-thopheneethylammonium iodide (TEAI), and phenethylammonium iodide (PEAI) were purchased from Greatcell Solar Materials. Cesium iodide (CsI), tin iodide (SnI_2), tin fluoride (SnF_2), 5-aminovaleric acid (5AVA), Sn powder, dimethyl sulfoxide (DMSO), dimethylformamide (DMF), chlorobenzene (CB), 2,2′,2″-(1,3,5-benzinetriyl)-tris(1-phenyl-1-*H*-benzimidazole) (TPBi), lithium fluoride (LiF), and molybdenum oxide (MoO_3) were purchased from Sigma-Aldrich. PEDOT:PSS and poly-TPD were purchased from Ossila and Lumtec, respectively.

MHP Film Deposition. The 0.11 M precursor was prepared as following this ratio: FAI:CsI:SnI$_2$:SnF$_2$:TEAI:5AVA = 0.9:0.1:1:0.15:0.3:0.15 in DMSO:DMF = 4:1 mixed solvent. The precursor solution was stirred at room temperature for 1 h to dissolve all precursors and then transferred into another vial with Sn powder (3 mg mL^{-1}). After stirring the Sn powder-contained precursor solution for 3 h, it was filtered by polytetrafluoroethylene with 0.45 μm pore size right before spin-coating. The filtered solution was spin-coated at 1000 rpm for 10 s, sequentially, at 7000 rpm for 60 s. The spin-coated sample was annealed at 65 °C for 25 min.

LED Device Fabrication. Prepatterned indium tin oxide (ITO) substrates were washed with detergent, deionized water, acetone, and isopropyl alcohol in order. The cleaned substrates were treated with an ultraviolet (UV) ozone cleaner for 20 min, and a diluted PEDOT:PSS (1:5 in deionized water) filtered by 0.45 μm polyvinylidene fluoride was spin-coated at 5000 rpm for 50 s onto the UV-treated substrate. The PEDOT:PSS/ITO substrates were heated at 150 °C for 10 min in air and dried again in a glovebox under the same condition. For ligand treatments, 0.02 M ligand solutions in DMF were spin-coated at 4000 rpm for 60 s, and the samples were dried at 100 °C for 10 min. After MHP film deposition, TPBi (45 nm), LiF (1.2 nm), and Al (100 nm) were deposited by a thermal evaporator. For a hole-only device, poly-TPD 10 mg mL^{-1} in CB was spin-coated at 4000 rpm for 30 s after the MHP film deposition, and then MoO_3 (10 nm) and Au (50 nm) were deposited by the thermal evaporator.

CHARACTERIZATION

NMR Spectra. NMR spectra were acquired with a Bruker AV 400-MHz spectrometer at room temperature with dimethyl sulfoxide-d6 (d-DMSO) as the solvent and tetramethylsilane (TMS) as the internal standard.

Cyclic Voltammetry (CV). CV was conducted on a CHI660 workstation with a three-electrode setup. Glassy carbon was used as the working electrode, Ag/AgCl was used as the reference electrode, and a Pt coil was used as the counter electrode; the electrolyte was 0.1 M TBAPF6 in dichloromethane. The reference electrode was calibrated by ferrocene redox. The measurement was conducted in a N_2 purged environment and with a scan rate of 40 mV/s.

Mass Spectrometry. High-resolution mass spectrometry was acquired in positive electrospray ionization (ESI) mode on an LTQ Orbitrap XL instrument.

Ultraviolet and X-ray Photoelectron Spectroscopy (UPS and XPS). XPS was conducted under a PHI 5600 ultrahigh vacuum system with a hemispherical electron energy analyzer. The excitation source was Mg Kα (1253.6 eV) with a PHI 04−548 dual anode X-ray source. UPS was obtained with a negative bias of 5 V, using a H Lyman-α photon source (E-LUX 121) with a photon energy of 10.2 eV.

Atomic Force Microscopy (AFM) and Kelvin Probe Force Microscopy (KPFM). AFM and contact potential difference (CPD) images were measured by an Asylum Research Cypher ES Environmental AFM. Three-dimensional (3D) height profiles were obtained with Park Systems NX-10.

Space-Charge-Limited Current (SCLC) and Device Characterization. Current density versus voltage was obtained by forward bias at a rate of 0.1 V s^{-1} by using a Keithyley 2450. Radiance, EL spectra, and operational stability were measured by LQ-100X from Enli Technology with a 100 mm integrating sphere. All device measurements were conducted in a N_2 glovebox at room temperature.

X-ray Diffraction (XRD). XRD pattern was obtained using Rigaku Smart Lab with a Cu Kα source.

Scanning Electron Microscope (SEM). Hitachi S-4800 field emission SEM was used to collect the SEM images.

Photoluminescence (PL) and Absorption Spectra, and Time-Resolved Photoluminescence (TRPL). For PL spectra, X-Cite Series 120 REPL LAMP and SpectraPro HRS-300 spectrometer were used as a light source and detector with a bandpass filter (330−385 nm) and dichroic mirror with a 400 nm cutoff to split light. Absorption spectra were collected by an Agilent UV−vis−NIR Cary-5000 spectrometer with transmission mode. For TRPL measurements, the excitation pump influence was 0.285 μJ/cm^2 with a picosecond pulse laser (Pico-Quant, LDH−P-C-450B) of 490 nm. The excitation light was focused using 20×, NA = 0.45 objective, and PL was detected by a single-photon counting module (PicoQuant) and a single-photon avalanche diode with a time resolution of 64 ps.

In Situ Grazing-Incidence Wide-Angle X-ray Scattering (GIWAXS). In situ GIWAXS spectra were taken at beamline 7.3.3. at the Advanced Light Source (ALS) at Lawrence Berkeley National Lab utilizing an incident wavelength of 10 keV and a custom-built multimodal spin coating system.[33] Experiments were done using an incident angle of 0.16° and a spin speed of 4000 rpm and taking 0.145 s exposure with a 5 ms detector read-out time for a duration of 3 min. The next 20 min exposures were taken every 5 s to capture longer-dynamic changes. The 2D spectra were recorded with a Pilatus 2M-2D detector and integrated along the scattering vector (q) to reduce to 1D with the NIKA GIWAXS software.

RESULTS AND DISCUSSION

In a device structure of Sn-based PeLEDs, ITO/PEDOT:PSS/$FASnI_3$/TPBi/LiF/Al, ligand treatment was applied between

https://doi.org/10.1021/acsphotonics.4c01467
ACS Photonics 2024, 11, 4941−4947

the PEDOT:PSS and Sn perovskite layers (Scheme 1). The PEDOT:PSS layer, which is hygroscopic and strongly acidic, can cause Sn oxidation in the Sn perovskite layer.[34] Our objective was to improve the device performance of Sn-based PeLEDs by increasing the chemical stability of the Sn perovskite layer through the ligand treatment at the interface. To systematically compare the effects of the ligand treatment, PEA, a conventional organic ligand; 4Tm, a p-type organic conjugated ligand previously shown to be effective between perovskite and hole transport layers;[35] and EDOT, newly synthesized for this study, were examined (Scheme 1b). Specifically, EDOT, containing a monomer of PEDOT, was used to enhance interfacial compatibility due to its molecular similarity to the PEDOT:PSS layer (highlighted in Scheme 1). Additionally, EDOT has a shallow highest occupied molecular orbital (HOMO) level compared to that of 4Tm due to the electron-rich structure (Figure 1a). The HOMO levels obtained from CV are −5.38 eV for 4Tm and −5.23 eV for EDOT, closely matching −5.2 eV of the PEDOT:PSS layer (Figure S1). PEA has a deeper HOMO level regarded as an insulating layer. The energy levels of the Sn perovskite layers with ligand treatment are similar (Figure 1b,c). The minor differences might occur due to mixtures of dimensionality from the ligand treatment, not having a perfect 3D phase. On the other hand, the valence band maximum (VBM) of the untreated Sn perovskite layer (control) is calculated to be −5.89 eV, much deeper than expected, likely due to Sn oxidation (Figure S2).

Scheme 1. Molecular Structures of (a) PEDOT:PSS and (b) Three Different Organic Ligands (PEA, 4Tm, and EDOT) for the Ligand Treatment in a Device Architecture of Sn-Based PeLEDs

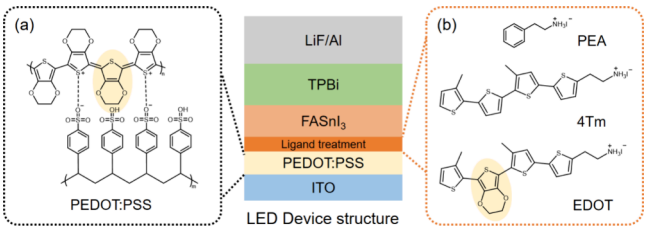

From a morphological perspective, grain sizes increase in EDOT-treated, 4Tm-treated, and PEA-treated films compared to those in the control film (Figure 2). As the size of island-type grains increases, the thickness of the Sn perovskite films also slightly increases, ranging from 80 to 100 nm (Figures S3 and S4). The 4Tm-treated and PEA-treated films exhibit higher intensity in XRD patterns corresponding to their larger grain size; however, these films have lower size uniformity compared to the control and EDOT-treated films (Figure S5). This uneven size distribution is detrimental to efficient charge injection and color purity due to nonuniform charge balance within the PeLED devices.[36] The nonuniform sizes of the 4Tm-treated and PEA-treated films can be attributed to high surface roughness from the ligand treatment on the PEDOT:PSS layer. The root-mean-square (RMS) roughness values for the untreated, EDOT-treated, 4Tm-treated, and PEA-treated films are 0.77 0.47, 1.62, and 2.41 nm, respectively. The higher roughness values for the 4Tm-treated and PEA-treated films indicate nonuniform nucleation sites during the crystallization process (Figure S6).[37] KPFM images reveal distinct differences in CPDs inside of the grains and at the surfaces for the 4Tm-treated and PEA-treated films (Figure 2c,d), while the control and EDOT-treated films have relatively uniform CPDs (Figure 2a,b). The 4Tm-treated and PEA-treated films are expected to have numerous defects interior of the grains compared to the control and EDOT-treated films, as indicated by the band bending associated with the defects.[38] This suggests that the ligand treatment can increase grain size and thickness; however, it may also introduce more defects and nonuniformity of the grain sizes.

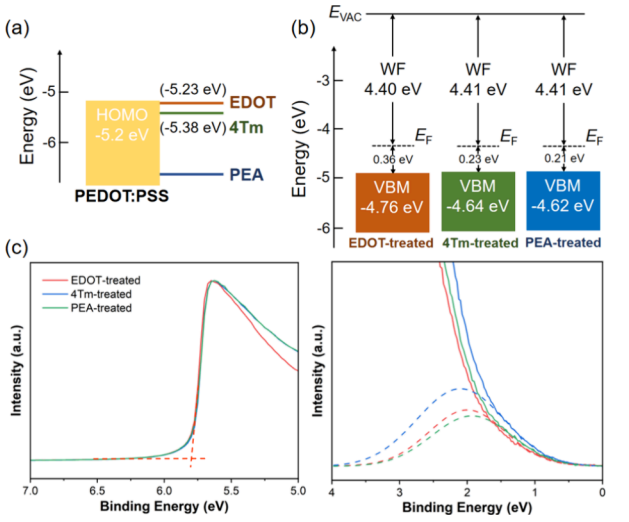

Figure 1. (a) Energy level diagram of EDOT, 4Tm, and PEA organic ligands with PEDOT:PSS. (b) Energy level scheme of the EDOT, 4Tm, and PEA-treated Sn perovskite films. Note that E_{VAC}, WF, and E_F are the vacuum level, work function, and Fermi level, respectively. (c) UPS spectra of the EDOT, 4Tm, and PEA-treated Sn perovskite films in the secondary electron cut off region (left) and the valence band region (right) measured with a source energy of 10.2 eV.

Sn oxidation is a common issue in Sn perovskite materials and is a primary factor contributing to the low chemical stability and device performance of Sn-based PeLEDs.[39,40] The degree of Sn oxidation in each film can be assessed by examining the Sn 3d peak in the XPS spectra. The control film displays a shift to higher binding energy compared to other ligand-treated films, indicating a higher degree of Sn^{4+} (Figure 3a and Figure S7). In other words, ligand treatment at the PEDOT:PSS interface effectively mitigates Sn oxidation regardless of the type of organic ligands. Thus, the application of appropriate ligand treatments can significantly enhance the chemical stability and device performance of Sn-based PeLEDs by preventing Sn oxidation.

Organic ligands can form quasi-two-dimensional (quasi-2D) perovskites with various <*n*> values, which are thicknesses of metal halide octahedral layers. The control film inherently contains 30% TEA ligand, and the additional ligands can participate in quasi-2D perovskites in the ligand-treated films. The dimensionality of the Sn perovskite films can be compared by analyzing emission wavelength in PL and absorption spectra due to the quantum confinement effect.[26] Although the ligand treatment was applied at the bottom interface, no significant difference is observed in the PL spectra between the top and bottom sides of the ligand-treated films with a single emission near ∼870 nm (Figure S8). The single emission visible at room temperature is attributed to the energy transfer from high *n* numbers to the 3D phase. To accurately compare the

https://doi.org/10.1021/acsphotonics.4c01467
ACS Photonics 2024, 11, 4941−4947

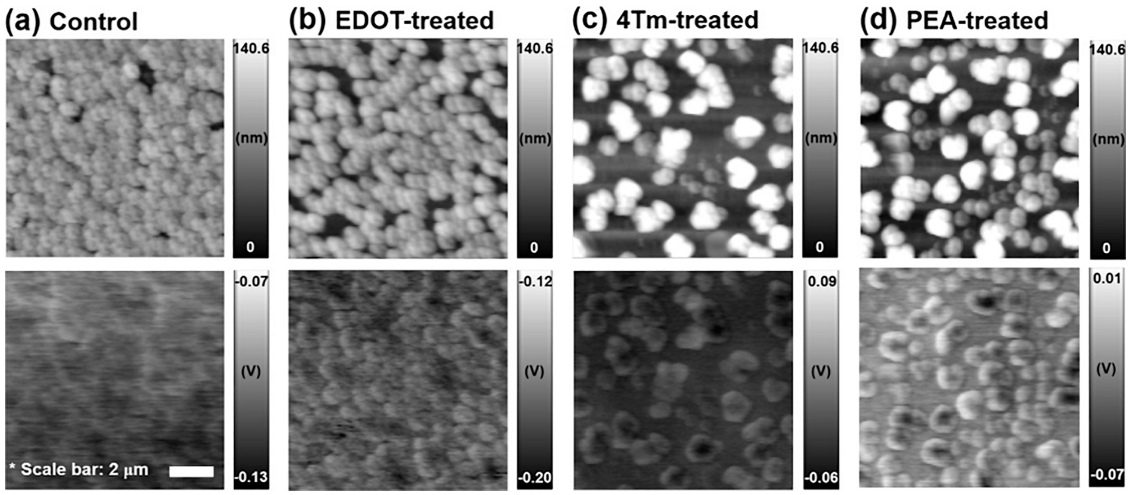

Figure 2. AFM (top) and KPFM (bottom) images of (a) control, (b) EDOT, (c) 4Tm, and (d) PEA-treated Sn perovskite films.

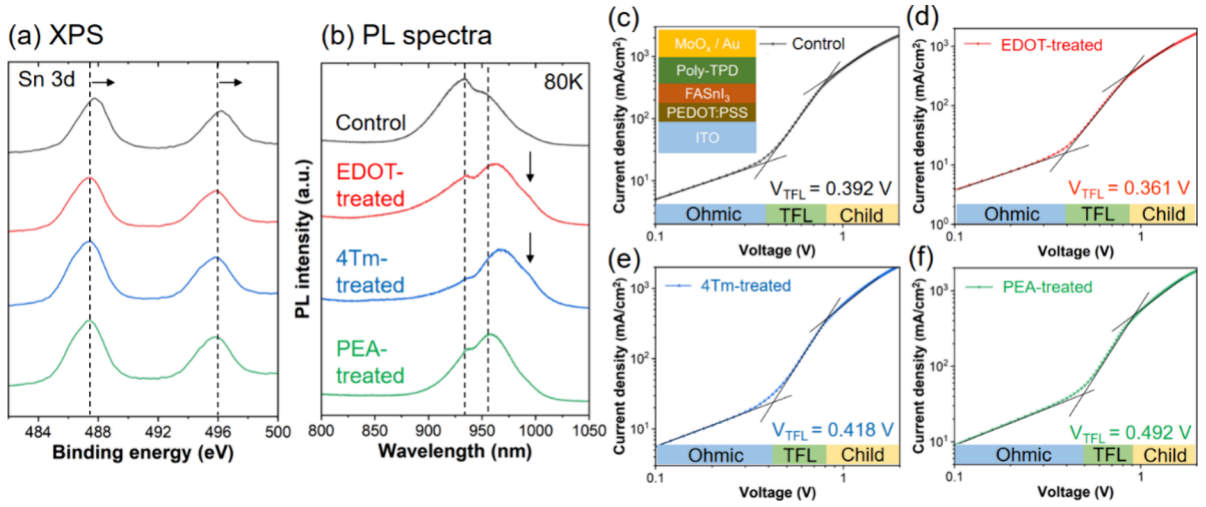

Figure 3. (a) XPS spectra of Sn 3d and (b) PL spectra for the control, EDOT, 4Tm, and PEA-treated Sn perovskite films. SCLC curves of the hole-only devices using (c) control, (d) EDOT, (e) 4Tm, and (f) PEA-treated Sn perovskite films.

dimensionality, PL spectra were examined at low temperatures, where energy transfer is limited (Figure 3b). As the temperature decreases, $FASnI_3$ perovskite films show a red shift due to the phase transition,[41,42] while quasi-2D perovskites generally exhibit a blue shift due to restricted energy transfer.[43] In this system, energy transfer from high n numbers to the 3D phase results in a red shift, consistent with the trend of $FASnI_3$ (Figure S9). The low-temperature PL spectra reveal two or three peaks: the 1000 nm emission corresponds to the 3D phase, while the 930−970 nm peaks indicate high n numbers (Figure 3b).[41,42] The EDOT-treated and 4Tm-treated films show higher $< n >$ values of the high n numbers than the control and PEA-treated films. Note that the two dashed lines in Figure 3b indicate the high n values in the control film. Furthermore, energy transfer to the 3D phase happens in the EDOT-treated and 4Tm-treated films even at 80K (arrow in Figure 3b), with more efficient energy funneling than in the control and PEA-treated films. In addition, absorption spectra suggest the presence of a minor $n = 2$ phase (Figure S10a). The $n = 2$ phase becomes more pronounced in PL mapping at a higher precursor concentration (0.22M) with enclosing the island-type grains (Figure S10b,c). This PL and absorption spectra suggest that a small amount of $n = 2$ phase surrounds the grains. This suggests that the organic ligands partially exist at the surfaces as the $n = 2$ phase and another form of high n numbers coexists with the 3D phase. In situ GIWAXS analysis further supports that the EDOT treatment results in various intermediate phases during the initial crystallization, eventually leading to many high n numbers in the final film compared to those in the control film (Figures S11 and S12). Unlike the control film with the dominant 3D phase and a flat energy landscape,[44] the EDOT-treated film exhibits stable 3D emission through efficient energy funneling, resulting in improved PLQY (Figure S13).

To evaluate the effect of the ligand treatment among the PEDOT:PSS, a hole injection layer, and the Sn perovskite films, the SCLC characteristics for hole-only devices were examined (Figure 3c−f). The EDOT-treated hole-only device shows a reduction in trap-filled limited voltage (V_{TFL}) from 0.392 V (the control) to 0.361 V, implying that the trap density decreases. In contrast, the 4Tm-treated and PEA-treated hole-only devices exhibit high V_{TFL} rising to 0.418 and 0.492 V, respectively. Although the 4Tm and PEA treatments can enhance the chemical stability of the Sn perovskite film compared to the control film, their mismatched energy levels lead to inefficient charge injection (Figure 1), and the inherent

https://doi.org/10.1021/acsphotonics.4c01467
ACS Photonics 2024, 11, 4941−4947

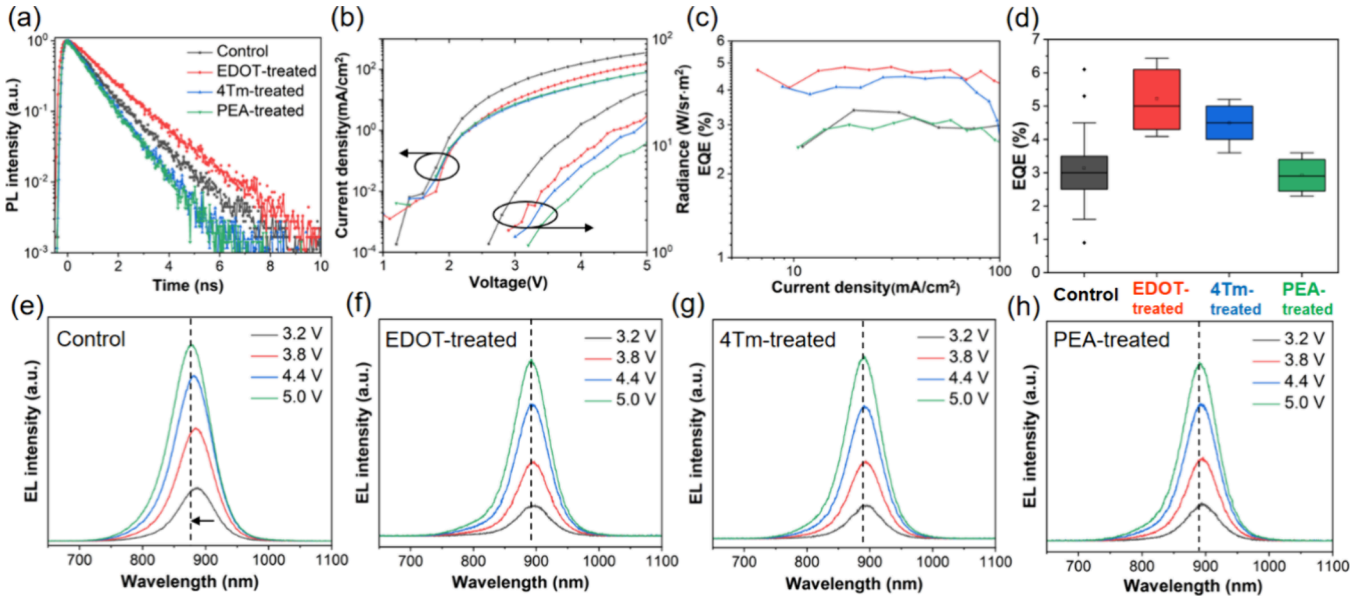

Figure 4. (a) TRPL decay curves of the Sn perovskite films with and without the ligand treatment. (b) Current density−voltage−radiance curves and (c) EQE characteristic of the control, EDOT, 4Tm, and PEA-treated Sn-based PeLEDs. (d) EQE statistics measured from the total 53 devices. Voltage-dependent EL spectra of the (e) control, (f) EDOT, (g) 4Tm, and (h) PEA-treated Sn-based PeLEDs.

defect density of the films increases (Figure 2), resulting in higher trap densities in the hole-only devices. TRPL measurements support these findings, showing that the EDOT-treated film has the longest carrier lifetime, followed by the control, 4Tm-treated, and PEA-treated films (Figure 4a).

To assess the impact of the ligand treatment on Sn-based PeLED devices, various optimization processes were conducted, followed by ligand treatment (Figures S14 and S15). In the optimized Sn-based PeLEDs, the current density−voltage−radiance curves show a reduction in current levels due to ligand treatment (Figure 4b). 4Tm and PEA-treated PeLEDs have higher turn-on voltages than the EDOT-treated PeLED because the energy mismatch between HOMO levels of the ligands and PEDOT:PSS layer leads to inefficient charge injection. The EDOT and 4Tm ligand treatments improve the EQE by aiding charge balance in the strong p-type Sn perovskite film (Figure 4c).[45] The average and maximum EQEs of the EDOT-treated PeLEDs are 5.22 and 6.44%, while the average EQEs of the control, 4Tm, and PEA-treated PeLEDs are 3.14%, 4.49%, and 2.93%, respectively (Figure 4d). Furthermore, the stability of the EL spectra at high voltages is enhanced; the EL spectra of the control PeLED are shifted from an emission wavelength of 890 nm at 3.2 V to 875 nm at 5 V (Figure 4e), whereas the ligand-treated PeLEDs exhibit negligible shifts (Figure 4f−h). This shift can be attributed to relatively low $\langle n \rangle$ values in the high n numbers, shown in Figure 3b. The EDOT treatment suggests enhanced oxidation stability and reduced defect density, leading to the reproduction of stable EL spectra and achieving the highest efficiency with an EQE of 6.4% in the PeLEDs.

CONCLUSIONS

This study demonstrates the significant impact of ligand treatment on the device performance of Sn-based PeLEDs. By introducing a newly designed EDOT-based conjugated organic ligand, we were able to prevent Sn oxidation and reduce the defect density of the Sn perovskite layer. These improvements lead to a high EQE of 6.4% and stable EL spectra in the EDOT-treated Sn-based PeLEDs. The findings suggest that a careful molecular design and appropriate ligand treatment are crucial for developing efficient and stable Sn-based PeLEDs, guiding future research in this promising field.

ASSOCIATED CONTENT

Supporting Information

The Supporting Information is available free of charge at https://pubs.acs.org/doi/10.1021/acsphotonics.4c01467.

Additional data on materials synthesis and additional characterization in respect of ^{1}H NMR, UPS, T-dependent PL, absorbance, and EL spectra, AFM, SEM, and GIWAXS images, XRD pattern, CV, $J-V-R$, and EQE−J curves, PLQY, and operational stability (PDF)

AUTHOR INFORMATION

Corresponding Author

Letian Dou − *Davidson School of Chemical Engineering, Department of Chemistry, and Birck Nanotechnology Center, Purdue University, West Lafayette, Indiana 47907, United States;* orcid.org/0000-0001-6411-8591; Email: dou10@purdue.edu

Authors

Seok Joo Yang − *Davidson School of Chemical Engineering, Purdue University, West Lafayette, Indiana 47907, United States; Department of Chemical Engineering, Kumoh National Institute of Technology, Gumi 39177, Republic of Korea*

Dharini Varadharajan − *Davidson School of Chemical Engineering, Purdue University, West Lafayette, Indiana 47907, United States*

Kagachi Tateno − *Davidson School of Chemical Engineering, Purdue University, West Lafayette, Indiana 47907, United States*

https://doi.org/10.1021/acsphotonics.4c01467
ACS Photonics 2024, 11, 4941−4947

Yu-Ting Yang − *Davidson School of Chemical Engineering, Purdue University, West Lafayette, Indiana 47907, United States*
Jeong Hui Kim − *Davidson School of Chemical Engineering, Purdue University, West Lafayette, Indiana 47907, United States*
Kevin R. Pedersen − *Department of Chemistry, University of Kentucky, Lexington, Kentucky 40506, United States*
Sung-Doo Baek − *Davidson School of Chemical Engineering, Purdue University, West Lafayette, Indiana 47907, United States*
Hanjun Yang − *Davidson School of Chemical Engineering and Department of Chemistry, Purdue University, West Lafayette, Indiana 47907, United States;* orcid.org/0000-0002-6856-6559
Aidan H. Coffey − *Advanced Light Source, Lawrence Berkeley National Lab, Berkeley, California 94720, United States*
Kenneth R. Graham − *Department of Chemistry, University of Kentucky, Lexington, Kentucky 40506, United States;* orcid.org/0000-0002-6387-3998
Bryan W. Boudouris − *Davidson School of Chemical Engineering and Department of Chemistry, Purdue University, West Lafayette, Indiana 47907, United States;* orcid.org/0000-0003-0428-631X

Complete contact information is available at: https://pubs.acs.org/10.1021/acsphotonics.4c01467

Author Contributions

[§]S.J.Y., D.V., and K.T. contributed equally.

Funding

This work is supported by the National Science Foundation (grant no. 2131608-ECCS).

Notes

The authors declare no competing financial interest.

REFERENCES

(1) Cao, Y.; Wang, N.; Tian, H.; Guo, J.; Wei, Y.; Chen, H.; Miao, Y.; Zou, W.; Pan, K.; He, Y.; Cao, H.; Ke, Y.; Xu, M.; Wang, Y.; Yang, M.; Du, K.; Fu, Z.; Kong, D.; Dai, D.; Jin, Y.; Li, G.; Li, H.; Peng, Q.; Wang, J.; Huang, W. Perovskite Light-Emitting Diodes Based on Spontaneously Formed Submicrometre-Scale Structures. *Nature* **2018**, *562*, 249−253.
(2) Chen, Z.; Zhang, C.; Jiang, X.-F.; Liu, M.; Xia, R.; Shi, T.; Chen, D.; Xue, Q.; Zhao, Y.-J.; Su, S.; Yip, H.-L.; Cao, Y. High-Performance Color-Tunable Perovskite Light Emitting Devices through Structural Modulation from Bulk to Layered Film. *Adv. Mater.* **2017**, *29*, 1603157.
(3) Xing, G.; Mathews, N.; Sun, S.; Lim, S. S.; Lam, Y. M.; Grätzel, M.; Mhaisalkar, S.; Sum, T. C. Long-Range Balanced Electron- and Hole-Transport Lengths in Organic-Inorganic $CH_3NH_3PbI_3$. *Science* **2013**, *342*, 344−347.
(4) Han, T.-H.; Jang, K. Y.; Dong, Y.; Friend, R. H.; Sargent, E. H.; Lee, T.-W. A roadmap for the commercialization of perovskite light emitters. *Nat. Rev. Mater.* **2022**, *7*, 757−777.
(5) Zhu, L.; Cao, H.; Xue, C.; Zhang, H.; Qin, M.; Wang, J.; Wen, K.; Fu, Z.; Jiang, T.; Xu, L.; Zhang, Y.; Cao, Y.; Tu, C.; Zhang, J.; Liu, D.; Zhang, G.; Kong, D.; Fan, N.; Li, G.; Yi, C.; Peng, Q.; Chang, J.; Lu, X.; Wang, N.; Huang, W.; Wang, J. Unveiling the Additive-Assisted Oriented Growth of Perovskite Crystallite for High Performance Light-Emitting Diode. *Nat. Commun.* **2021**, *12*, 5081.
(6) Hassan, Y.; Park, J. H.; Crawford, M. L.; Sadhanala, A.; Lee, J.; Sadighian, J. C.; Mosconi, E.; Shivanna, R.; Radicchi, E.; Jeong, M.; Yang, C.; Choi, H.; Park, S. H.; Song, M. H.; De Angelis, F.; Wong, C. Y.; Friend, R. H.; Lee, B. R.; Snaith, H. J. Ligand-Engineered Bandgap Stability in Mixed-Halide Perovskite LEDs. *Nature* **2021**, *591*, 72−77.
(7) Ma, D.; Lin, K.; Dong, Y.; Choubisa, H.; Proppe, A. H.; Wu, D.; Wang, Y.-K.; Chen, B.; Li, P.; Fan, J. Z.; Yuan, F.; Johnston, A.; Liu, Y.; Kang, Y.; Lu, Z.-H.; Wei, Z.; Sargent, E. H. Distribution Control Enables Efficient Reduced-Dimensional Perovskite LEDs. *Nature* **2021**, *599*, 594−598.
(8) Kong, L.; Sun, Y.; Zhao, B.; Ji, K.; Feng, J.; Dong, J.; Wang, Y.; Liu, Z.; Maqbool, S.; Li, Y.; Yang, Y.; Dai, L.; Lee, W.; Cho, C.; Stranks, S. D.; Friend, R. H.; Wang, N.; Greenham, N. C.; Yang, X. Fabrication of Red-Emitting Perovskite LEDs by Stabilizing Their Octahedral Structure. *Nature* **2024**, *631*, 73−79.
(9) Yang, X.; Zhang, X.; Deng, J.; Chu, Z.; Jiang, Q.; Meng, J.; Wang, P.; Zhang, L.; Yin, Z.; You, J. Efficient Green Light-Emitting Diodes Based on Quasi-Two-Dimensional Composition and Phase Engineered Perovskite with Surface Passivation. *Nat. Commun.* **2018**, *9*, 1169.
(10) Wang, Q.; Wang, X.; Yang, Z.; Zhou, N.; Deng, Y.; Zhao, J.; Xiao, X.; Rudd, P.; Moran, A.; Yan, Y.; Huang, J. Efficient Sky-Blue Perovskite Light-Emitting Diodes via Photoluminescence Enhancement. *Nat. Commun.* **2019**, *10*, 5633.
(11) Pan, Z.; Lu, Y.-Y.; Liu, F. Sunlight-Activated Long-Persistent Luminescence in the Near-Infrared from Cr^{3+}-Doped Zinc Gallogermanates. *Nat. Mater.* **2012**, *11*, 58−63.
(12) Chen, S.; Weitemier, A. Z.; Zeng, X.; He, L.; Wang, X.; Tao, Y.; Huang, A. J. Y.; Hashimotodani, Y.; Kano, M.; Iwasaki, H.; Parajuli, L. K.; Okabe, S.; Teh, D. B. L.; All, A. H.; Tsutsui-Kimura, I.; Tanaka, K. F.; Liu, X.; McHugh, T. J. Near-Infrared Deep Brain Stimulation via Upconversion Nanoparticle−Mediated Optogenetics. *Science* **2018**, *359*, 679−684.
(13) Michalet, X.; Pinaud, F. F.; Bentolila, L. A.; Tsay, J. M.; Doose, S.; Li, J. J.; Sundaresan, G.; Wu, A. M.; Gambhir, S. S.; Weiss, S. Quantum Dots for Live Cells, in Vivo Imaging, and Diagnostics. *Science* **2005**, *307*, 538−544.
(14) Xie, C.; Zhao, X.; Ong, E. W. Y.; Tan, Z.-K. Transparent Near-Infrared Perovskite Light-Emitting Diodes. *Nat. Commun.* **2020**, *11*, 4213.
(15) Qiu, W.; Xiao, Z.; Roh, K.; Noel, N. K.; Shapiro, A.; Heremans, P.; Rand, B. P. Mixed Lead−Tin Halide Perovskites for Efficient and Wavelength-Tunable Near-Infrared Light-Emitting Diodes. *Adv. Mater.* **2019**, *31*, 1806105.
(16) Wang, K.; Jin, L.; Gao, Y.; Liang, A.; Finkenauer, B. P.; Zhao, W.; Wei, Z.; Zhu, C.; Guo, T.-F.; Huang, L.; Dou, L. Lead-Free Organic−Perovskite Hybrid Quantum Wells for Highly Stable Light-Emitting Diode. *ACS Nano* **2021**, *15*, 6316−6325.
(17) Yakunin, S.; Benin, B. M.; Shynkarenko, Y.; Nazarenko, O.; Bodnarchuk, M. I.; Dirin, D. N.; Hofer, C.; Cattaneo, S.; Kovalenko, M. V. High-Resolution Remote Thermometry and Thermography Using Luminescent Low-Dimensional Tin-Halide Perovskites. *Nat. Mater.* **2019**, *18*, 846−852.
(18) Hong, W.-L.; Huang, Y.-C.; Chang, C.-Y.; Zhang, Z.-C.; Tsai, H.-R.; Chang, N.-Y.; Chao, Y.-C. Efficient Low-Temperature Solution-Processed Lead-Free Perovskite Infrared Light-Emitting Diodes. *Adv. Mater.* **2016**, *28*, 8029−8036.
(19) Li, J.; Cao, H.-L.; Jiao, W.-B.; Wang, Q.; Wei, M.; Cantone, I.; Lü, J.; Abate, A. Biological Impact of Lead from Halide Perovskites Reveals the Risk of Introducing a Safe Threshold. *Nat. Commun.* **2020**, *11*, 310.
(20) Lu, J.; Guan, X.; Li, Y.; Lin, K.; Feng, W.; Zhao, Y.; Yan, C.; Li, M.; Shen, Y.; Qin, X.; Wei, Z. Dendritic $CsSnI_3$ for Efficient and Flexible Near-Infrared Perovskite Light-Emitting Diodes. *Adv. Mater.* **2021**, *33*, No. 2104414.
(21) Zhang, F.; Min, H.; Zhang, Y.; Kuang, Z.; Wang, J.; Feng, Z.; Wen, K.; Xu, L.; Yang, C.; Shi, H.; Zhuo, C.; Wang, N.; Chang, J.; Huang, W.; Wang, J. Vapor-Assisted In Situ Recrystallization for Efficient Tin-Based Perovskite Light-Emitting Diodes. *Adv. Mater.* **2022**, *34*, 2203180.
(22) Yuan, F.; Zheng, X.; Johnston, A.; Wang, Y.-K.; Zhou, C.; Dong, Y.; Chen, B.; Chen, H.; Fan, J. Z.; Sharma, G.; Li, P.; Gao, Y.; Voznyy, O.; Kung, H.-T.; Lu, Z.-H.; Bakr, O. M.; Sargent, E. H.

Color-Pure Red Light-Emitting Diodes Based on Two-Dimensional Lead-Free Perovskites. *Sci. Adv.* **2020**, *6*, No. eabb0253.
(23) Dong, H.; Ran, C.; Gao, W.; Sun, N.; Liu, X.; Xia, Y.; Chen, Y.; Huang, W. Crystallization Dynamics of Sn-Based Perovskite Thin Films: Toward Efficient and Stable Photovoltaic Devices. *Adv. Energy Mater.* **2022**, *12*, 2102213.
(24) Jia, Y.-H.; Neutzner, S.; Zhou, Y.; Yang, M.; Tapia, J. M. F.; Li, N.; Yu, H.; Cao, J.; Wang, J.-P.; Petrozza, A.; Wong, C.-P.; Zhao, N. Role of Excess FAI in Formation of High-Efficiency $FAPbI_3$-Based Light-Emitting Diodes. *Adv. Funct. Mater.* **2020**, *30*, 1906875.
(25) Guo, Y.; Jia, Y.; Li, N.; Chen, M.; Hu, S.; Liu, C.; Zhao, N. Degradation Mechanism of Perovskite Light-Emitting Diodes: An In Situ Investigation via Electroabsorption Spectroscopy and Device Modelling. *Adv. Funct. Mater.* **2020**, *30*, 1910464.
(26) Yang, S. J.; Kim, D.; Choi, J.; Kim, S. H.; Park, K.; Ryu, S.; Cho, K. Enhancing Thermoelectric Power Factor of 2D Organometal Halide Perovskites by Suppressing 2D/3D Phase Separation. *Adv. Mater.* **2021**, *33*, 2102797.
(27) Wu, Y.; Wan, L.; Fu, S.; Zhang, W.; Li, X.; Fang, J. Liquid Metal Acetate Assisted Preparation of High-Efficiency and Stable Inverted Perovskite Solar Cells. *J. Mater. Chem. A* **2019**, *7*, 14136−14144.
(28) Jin, H.; Debroye, E.; Keshavarz, M.; Scheblykin, I. G.; Roeffaers, M. B. J.; Hofkens, J.; Steele, J. A. It's a Trap! On the Nature of Localised States and Charge Trapping in Lead Halide Perovskites. *Mater. Horiz.* **2020**, *7*, 397−410.
(29) Fang, Z.; Chen, W.; Shi, Y.; Zhao, J.; Chu, S.; Zhang, J.; Xiao, Z. Dual Passivation of Perovskite Defects for Light-Emitting Diodes with External Quantum Efficiency Exceeding 20%. *Adv. Funct. Mater.* **2020**, *30*, 1909754.
(30) Koh, T. M.; Krishnamoorthy, T.; Yantara, N.; Shi, C.; Leong, W. L.; Boix, P. P.; Grimsdale, A. C.; Mhaisalkar, S. G.; Mathews, N. Formamidinium Tin-Based Perovskite with Low E_g for Photovoltaic Applications. *J. Mater. Chem. A* **2015**, *3*, 14996−15000.
(31) Kumar, M. H.; Dharani, S.; Leong, W. L.; Boix, P. P.; Prabhakar, R. R.; Baikie, T.; Shi, C.; Ding, H.; Ramesh, R.; Asta, M.; Graetzel, M.; Mhaisalkar, S. G.; Mathews, N. Lead-Free Halide Perovskite Solar Cells with High Photocurrents Realized Through Vacancy Modulation. *Adv. Mater.* **2014**, *26*, 7122−7127.
(32) Gao, Y.; Shi, E.; Deng, S.; Shiring, S. B.; Snaider, J. M.; Liang, C.; Yuan, B.; Song, R.; Janke, S. M.; Liebman-Peláez, A.; Yoo, P.; Zeller, M.; Boudouris, B. W.; Liao, P.; Zhu, C.; Blum, V.; Yu, Y.; Savoie, B. M.; Huang, L.; Dou, L. Molecular engineering of organic-inorganic hybrid perovskites quantum wells. *Nat. Chem.* **2019**, *11*, 1151−1157.
(33) Coffey, A. H.; Slack, J.; Cornell, E.; Yang, L. L.; Anderson, K.; Wang, K.; Dou, L.; Zhu, C. In situ spin coater for multimodal grazing incidence x-ray scattering studies. *Rev. Sci. Instrum.* **2023**, *94*, No. 093906.
(34) Yang, S. J.; Choi, J.; Song, S.; Park, C.; Cho, K. Enhancing Air-Stability and Reproducibility of Lead-Free Formamidinium-Based Tin Perovskite Solar Cell by Chlorine Doping. *Sol. Energy Mater. Sol. Cells* **2021**, *227*, No. 111072.
(35) Ma, K.; Atapattu, H. R.; Zhao, Q.; Gao, Y.; Finkenauer, B. P.; Wang, K.; Chen, K.; Park, S. M.; Coffey, A. H.; Zhu, C.; Huang, L.; Graham, K. R.; Mei, J.; Dou, L. Multifunctional Conjugated Ligand Engineering for Stable and Efficient Perovskite Solar Cells. *Adv. Mater.* **2021**, *33*, 2100791.
(36) Ngai, K. H.; Sun, X.; Zou, X.; Fan, K.; Wei, Q.; Li, M.; Li, S.; Lu, X.; Meng, W.; Wu, B.; Zhou, G.; Long, M.; Xu, J. Charge Injection and Auger Recombination Modulation for Efficient and Stable Quasi-2D Perovskite Light-Emitting Diodes. *Adv. Sci.* **2024**, *11*, 2309500.
(37) Li, M.; Yan, X.; Kang, Z.; Liao, X.; Li, Y.; Zheng, X.; Lin, P.; Meng, J.; Zhang, Y. Enhanced Efficiency and Stability of Perovskite Solar Cells via Anti-Solvent Treatment in Two-Step Deposition Method. *ACS Appl. Mater. Interfaces* **2017**, *9*, 7224−7231.
(38) Yang, Y.; Wu, L.; Hao, X.; Tang, Z.; Lai, H.; Zhang, J.; Wang, W.; Feng, L. Beneficial effects of potassium iodide incorporation on grain boundaries and interfaces of perovskite solar cells. *RSC Adv.* **2019**, *9*, 28561−28568.
(39) Min, H.; Wang, N.; Chen, N.; Tong, Y.; Wang, Y.; Wang, J.; Liu, J.; Wang, S.; Wu, X.; Yang, P.; Shi, H.; Zhuo, C.; Chen, Q.; Li, J.; Zhang, D.; Lu, X.; Zhu, C.; Peng, Q.; Zhu, L.; Chang, J.; Huang, W.; Wang, J. Spin coating epitaxial heterodimensional tin perovskites for light-emitting diodes. *Nat. Nanotechnol.* **2024**, *19*, 632−637.
(40) Min, H.; Chang, J.; Tong, Y.; Wang, J.; Zhang, F.; Feng, Z.; Bi, X.; Chen, N.; Kuang, Z.; Wang, S.; Yuan, L.; Shi, H.; Zhao, N.; Qian, D.; Xu, S.; Zhu, L.; Wang, N.; Huang, W.; Wang, J. Additive treatment yields high-performance lead-free perovskite light-emitting diodes. *Nat. Photonics* **2023**, *17*, 755−760.
(41) Kahmann, S.; Nazarenko, O.; Shao, S.; Hordiichuk, O.; Kepenekian, M.; Even, J.; Kovalenko, M. V.; Blake, G. R.; Loi, M. A. Negative Thermal Quenching in $FASnI_3$ Perovskite Single Crystals and Thin Films. *ACS Energy Lett.* **2020**, *5*, 2512−2519.
(42) Kahmann, S.; Shao, S.; Loi, M. A. Cooling, Scattering, and Recombination − The Role of the Material Quality for the Physics of Tin Halide Perovskites. *Adv. Funct. Mater.* **2019**, *29*, 1902963.
(43) Yang, S. J.; Wang, K.; Luo, Y.; Park, J. Y.; Yang, H.; Coffey, A. H.; Ma, K.; Sun, J.; Wieghold, S.; Zhu, C.; Dou, L. Two-Factor Phase Separations in Mixed-Halide Quasi-2D Perovskite LEDs: Dimensionality and Halide Segregations. *ACS Energy Lett.* **2023**, *8*, 3693−3701.
(44) Quan, L. N.; Zhao, Y.; García de Arquer, F. P.; Sabatini, R.; Walters, G.; Voznyy, O.; Comin, R.; Li, Y.; Fan, J. Z.; Tan, H.; Pan, J.; Yuan, M.; Bakr, O. M.; Lu, Z.; Kim, D. H.; Sargent, E. H. Tailoring the Energy Landscape in Quasi-2D Halide Perovskites Enables Efficient Green-Light Emission. *Nano Lett.* **2017**, *17*, 3701−3709.
(45) Chowdhury, T. H.; Reo, Y.; Yusoff, A. R. B. M.; Noh, Y.-Y. Sn-Based Perovskite Halides for Electronic Devices. *Adv. Sci.* **2022**, *9*, 2203749.

https://doi.org/10.1021/acsphotonics.4c01467
ACS Photonics 2024, 11, 4941−4947